NUWC-NPT Technical Report 11,404
6 December 2002

A Method for Estimating the Mechanical Properties of a Solid Material Subjected to Insonification — Part I: Theory

Andrew J. Hull
Submarine Sonar Department

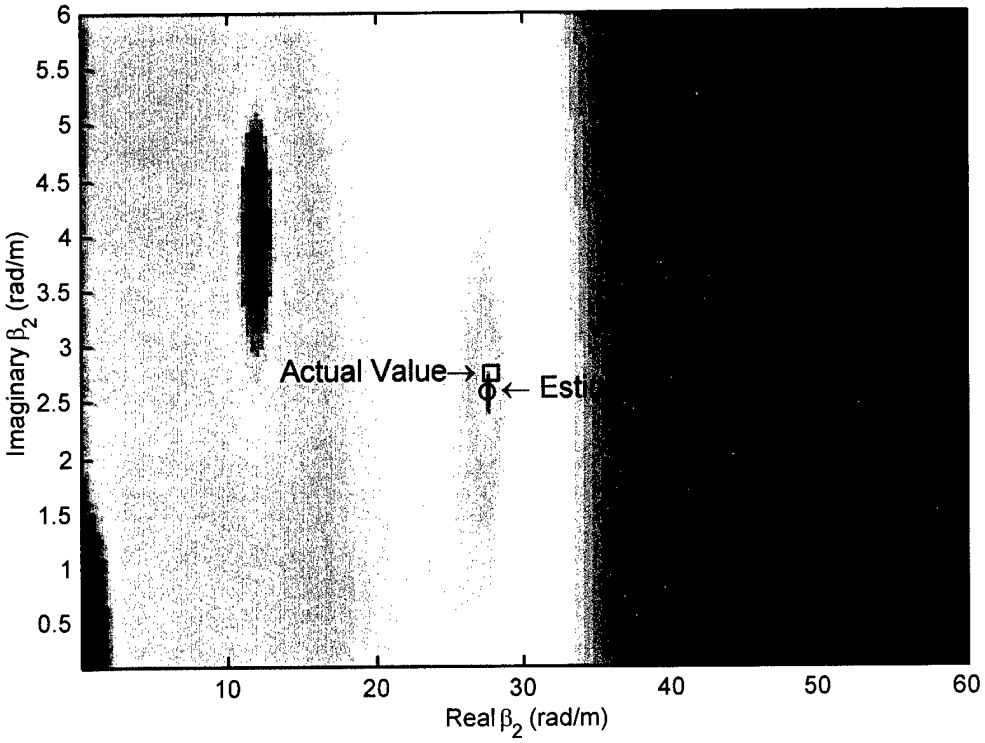

NAVSEA
NEWPORT
Undersea Warfare Center Division

Naval Undersea Warfare Center Division
Newport, Rhode Island

PREFACE

This report was prepared under NUWC Project No. 701Y070.

The technical reviewer was David A. Hurdis (Code 2141).

The author wishes to thank Karen Holt (Code 543) for her help with the editing of the manuscript.

Reviewed and Approved: 6 December 2002

Ronald J. Martin
Head, Submarine Sonar Department

The illustration on the front cover plots a simulated transfer function versus real and imaginary modified wavenumbers at 800 Hz. With the inverse method developed in this report, it is shown that the propagation wavenumbers can be estimated very accurately.

REPORT DOCUMENTATION PAGE

Form Approved
OMB No. 0704-0188

1. AGENCY USE ONLY *(Leave blank)*	2. REPORT DATE	3. REPORT TYPE AND DATES COVERED
	6 December 2002	

4. TITLE AND SUBTITLE

A Method for Estimating the Mechanical Properties of a Solid Material Subjected to Insonification — Part I: Theory

5. FUNDING NUMBERS

6. AUTHOR(S)

Andrew J. Hull

7. PERFORMING ORGANIZATION NAME(S) AND ADDRESS(ES)

Naval Undersea Warfare Center Division
1176 Howell Street
Newport, RI 02841-1708

8. PERFORMING ORGANIZATION REPORT NUMBER

TR 11,404

9. SPONSORING/MONITORING AGENCY NAME(S) AND ADDRESS(ES)

10. SPONSORING/MONITORING AGENCY REPORT NUMBER

11. SUPPLEMENTARY NOTES

12a. DISTRIBUTION/AVAILABILITY STATEMENT

Approved for public release; distribution is unlimited.

12b. DISTRIBUTION CODE

13. ABSTRACT (Maximum 200 words)

A theoretical inverse method is developed to measure the complex, frequency-dependent dilatational and shear wavespeeds that are present in isotropic thick plates. Once these wavespeeds are identified, the complex, frequency-dependent Young's and shear moduli and complex, frequency-dependent Poisson's ratio can be estimated. Simulations are presented both with and without noise to show how the method works and how the measurement error affects the analysis results.

14. SUBJECT TERMS

Insonification Techniques
Structural Stiffness/Loss
Mechanical Property Estimates
Thick Plate Theory

15. NUMBER OF PAGES
40

16. PRICE CODE

17. SECURITY CLASSIFICATION OF REPORT	18. SECURITY CLASSIFICATION OF THIS PAGE	19. SECURITY CLASSIFICATION OF ABSTRACT	20. LIMITATION OF ABSTRACT
Unclassified	Unclassified	Unclassified	SAR

TABLE OF CONTENTS

LIST OF ILLUSTRATIONS

LIST OF TABLES

A METHOD FOR ESTIMATING THE MECHANICAL PROPERTIES OF A SOLID MATERIAL SUBJECTED TO INSONIFICATION — PART I: THEORY

INTRODUCTION

Measurement of the mechanical properties of slab-shaped materials (i.e., plates) is important because of the significant contributions made by these properties to the static and dynamic response of a structure under various loading conditions.

Resonant techniques,[1-3] used to identify and measure Young's modulus for many years, have now been extended to measure the shear modulus of materials.[4] Such procedures are based on comparing the measured eigenvalues of a structure to those predicted from a model of the same structure formulated with well-defined (typically closed-form) eigenvalues. Resonant techniques allow measurements at resonant frequencies and, in general, utilize long, thin materials so that the waves propagate only in a longitudinal or torsional direction. The methods have also been extended to nonresonant frequencies,[3,5-7]which typically use one or more inverted transfer functions of thin-bar data to solve for Young's modulus. Other research has considered the bulk modulus of small-sized materials through the insonification of samples and the use of lasers to measure the resulting strain.[8]

Comparison of analytical models to measured frequency response functions[9-12] is yet another approach used to estimate the stiffness and loss parameters of a structure. When the analytical model agrees with one or more frequency response functions, the parameters used to calculate the analytical model are considered to be accurate. However, when the analytical model is formulated with a numerical method, comparing the model and the data can be difficult because of the dispersion properties of the materials. Moreover, if a single type of wave motion is dominant in the experiment, the parameters associated with secondary types of wave motion are unlikely to be estimated correctly.

Some investigators have concentrated on the stiffness and loss parameters of thin plates, with one method employing transmission zeros to calculate unknown coefficients at ultrasonic

frequencies[13] and a second using the natural frequencies of the plate to determine the elastic constants.[14] In addition, plate parameter estimation has been extended to measure experimental plate natural frequencies that are matched to a numerical simulation for estimating elastic constants.[15] Finally, studies of plate theory that relate transmission loss and reflection loss (echo reduction) to transfer functions across the plate have been made,[16] although this work does not contain a parameter estimation technique.

A theoretical inverse method to measure complex, frequency-dependent dilatational and shear wavespeeds that are present in thick, isotropic plates is developed in this report. After the linear equations of motion of the system are derived from thick plate theory, the inverse method is used to combine three transfer function measurements that yield closed-form values of the complex, frequency-dependent Young's and shear moduli and complex, frequency-dependent Poisson's ratio. Simulations are presented both with and without noise to show how the method works and how the measurement error affects the analysis results.

A typical test configuration, as seen in figure 1, uses a speaker to project acoustic energy onto the material. Intended for use when a plate is to undergo acoustic loading on its face, this technique can be applied to automobile, building, and submarine materials.

SYSTEM MODEL

As described above, the experiment consists of insonifying a slab-shaped test specimen by loading the structure on one entire side with an acoustic wave originating at the speaker. The speaker (or projector) is located at such a distance from the material that the acoustic wave nearly becomes a plane wave by the time it has established contact with the specimen. This type of experiment — usually conducted at multiple frequencies and multiple insonification angles — employs a frequency sweep (swept sine) at three different insonification angles for the inverse method presented here. During insonification, transfer function data are collected from both sides of the plate, either with accelerometers that measure accelerations or with laser velocimeters that use reflected light to measure velocities. In the swept-sine mode, transfer

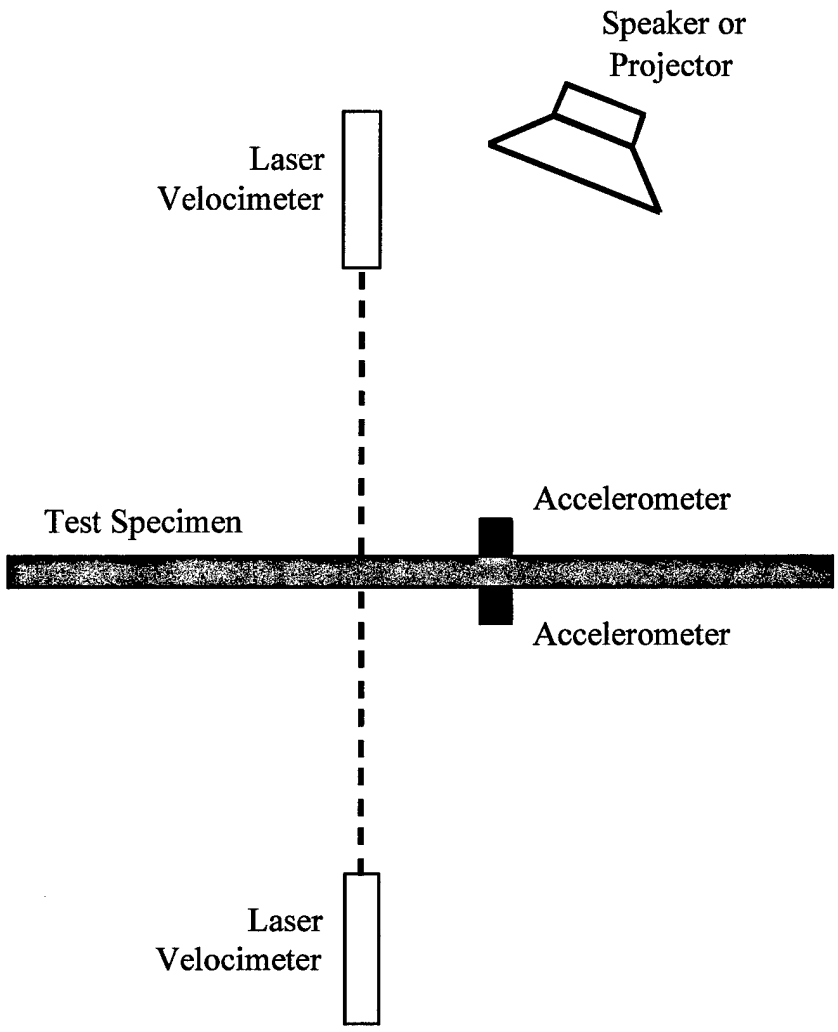

Figure 1. Test Configuration to Insonify and Measure Material

functions of acceleration divided by acceleration or velocity divided by velocity will be equal to displacement divided by displacement. Finally, the time domain data are Fourier transformed into the frequency domain and then recorded as complex transfer functions, typically with a spectrum analyzer.

The model and theoretical analysis are based on the following assumptions:

- the forcing function acting on the plate is a plane wave with definite wavenumber and frequency content;

- the corresponding response of the plate is at a definite wavenumber and frequency;
- motion is normal and tangential to the plate in one direction (two-dimensional system);
- the plate has an infinite spatial extent; and
- the particle motion is linear.

The motion of the test specimen shown in figure 1 is governed by the equation

$$\mu\nabla^2\mathbf{u} + (\lambda+\mu)\nabla\nabla\bullet\mathbf{u} = \rho\frac{\partial^2\mathbf{u}}{\partial t^2}\ , \tag{1}$$

where λ and μ are the complex Lamé constants ($\mathrm{N/m^2}$), ρ is the density ($\mathrm{kg/m^3}$), t is time (s), $\bullet$ denotes a vector dot product, and $\mathbf{u}$ is the Cartesian coordinate displacement vector of the material.

Figure 2 illustrates the coordinate system of the test configuration. Note that using this orientation results in $b = 0$ and a having a value that is less than zero, with the thickness of the specimen, h, exhibiting a positive value. Equation (1) is manipulated by writing the displacement vector $\mathbf{u}$ as

$$\mathbf{u} = \begin{Bmatrix} u_x(x,y,z,t) \\ u_y(x,y,z,t) \\ u_z(x,y,z,t) \end{Bmatrix}\ , \tag{2}$$

where x is the location along the plate (m), y is the location into the plate (m), and z is the location normal to the plate (m), as shown in the figure. The symbol ∇ is the gradient vector differential operator written in three-dimensional Cartesian coordinates as

$$\nabla = \frac{\partial}{\partial x}i_x + \frac{\partial}{\partial y}i_y + \frac{\partial}{\partial z}i_z\ , \tag{3}$$

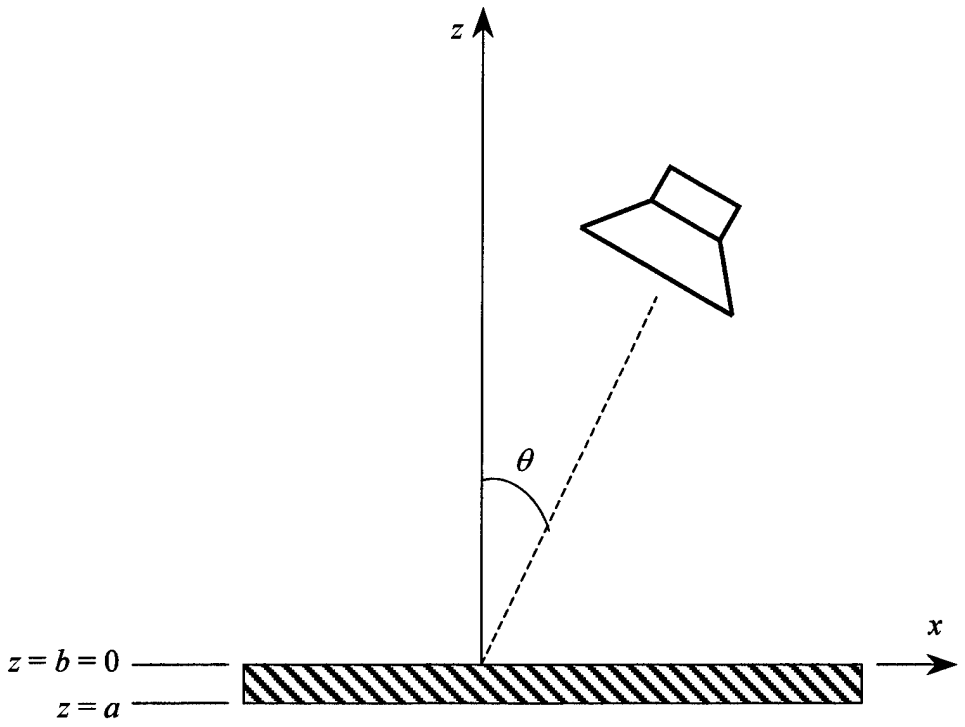

Figure 2. Coordinate System of the Test Configuration

with i_x denoting the unit vector in the x-direction, i_y denoting the unit vector in the y-direction, and i_z denoting the unit vector in the z-direction. The symbol ∇^2 is the three-dimensional Laplace operator applied to vector **u** as

$$\nabla^2 \mathbf{u} = \nabla^2 u_x i_x + \nabla^2 u_y i_y + \nabla^2 u_z i_z \tag{4}$$

and to scalar u as

$$\nabla^2 u_{x,y,z} = \nabla \bullet \nabla u_{x,y,z} = \frac{\partial^2 u_{x,y,z}}{\partial x^2} + \frac{\partial^2 u_{x,y,z}}{\partial y^2} + \frac{\partial^2 u_{x,y,z}}{\partial z^2} \ , \tag{5}$$

where the term $\nabla \bullet \mathbf{u}$ is the divergence and is equal to

$$\nabla \bullet \mathbf{u} = \frac{\partial u_x}{\partial x} + \frac{\partial u_y}{\partial y} + \frac{\partial u_z}{\partial z} \ . \tag{6}$$

The displacement vector **u** is written as

$$\mathbf{u} = \nabla\phi + \nabla \times \vec{\psi} \ , \tag{7}$$

where ϕ is a dilatational scalar potential, $\times$ denotes a vector cross product, and $\vec{\psi}$ is an equivoluminal vector potential expressed as

$$\vec{\psi} = \begin{Bmatrix} \psi_x(x,y,z,t) \\ \psi_y(x,y,z,t) \\ \psi_z(x,y,z,t) \end{Bmatrix} . \tag{8}$$

The problem is formulated as a two-dimensional system, and thus $y \equiv 0$, $u_y(x,y,z,t) \equiv 0$, and $\partial(\cdot)/\partial y \equiv 0$. Expanding equation (7) and breaking the displacement vector into its individual nonzero terms yields

$$u_x(x,z,t) = \frac{\partial\phi(x,z,t)}{\partial x} - \frac{\partial\psi_y(x,z,t)}{\partial z} \tag{9}$$

and

$$u_z(x,z,t) = \frac{\partial\phi(x,z,t)}{\partial z} + \frac{\partial\psi_y(x,z,t)}{\partial x} \ . \tag{10}$$

Equations (9) and (10) are next inserted into equation (1), which results in

$$c_d^2\nabla^2\phi(x,z,t) = \frac{\partial^2\phi(x,z,t)}{\partial t^2} \tag{11}$$

and

$$c_s^2\nabla^2\psi_y(x,z,t) = \frac{\partial^2\psi_y(x,z,t)}{\partial t^2} \ , \tag{12}$$

where equation (11) corresponds to the dilatational component and equation (12) corresponds to the shear component of the displacement field. Correspondingly, the constants c_d and c_s are the complex dilatational and shear wavespeeds, respectively, and are determined by

$$c_d = \sqrt{\frac{\lambda + 2\mu}{\rho}} \tag{13}$$

and

$$c_s = \sqrt{\frac{\mu}{\rho}} \ . \tag{14}$$

The relationship of the Lamé constants to the Young's and shear moduli is shown as

$$\lambda = \frac{E\upsilon}{(1+\upsilon)(1-2\upsilon)} \tag{15}$$

and

$$\mu = G = \frac{E}{2(1+\upsilon)} \ , \tag{16}$$

where E is the complex Young's modulus ($\mathrm{N/m^2}$), G is the complex shear modulus ($\mathrm{N/m^2}$), and υ is the Poisson's ratio of the material (dimensionless).

The conditions of infinite length and steady-state response are now imposed, allowing the scalar and vector potential to be written as

$$\phi(x,z,t) = \Phi(z)\exp(\mathrm{i}kx)\exp(\mathrm{i}\omega t) \tag{17}$$

and

$$\psi_y(x,z,t) = \Psi(z)\exp(\mathrm{i}kx)\exp(\mathrm{i}\omega t)\,, \tag{18}$$

where i is the square root of -1, ω is the frequency (rad/s), and k is the wavenumber with respect to the x-axis (rad/m). Inserting equation (17) into equation (11) yields

$$\frac{d^2\Phi(z)}{dz^2} + \alpha^2\Phi(z) = 0 \ , \tag{19}$$

where

$$\alpha = \sqrt{k_d^2 - k^2} \ , \tag{20}$$

with

$$k_d = \frac{\omega}{c_d} \ . \tag{21}$$

Inserting equation (18) into equation (12) yields

$$\frac{d^2\Psi(z)}{dz^2} + \beta^2\Psi(z) = 0 \ , \tag{22}$$

where

$$\beta = \sqrt{k_s^2 - k^2} \ , \tag{23}$$

with

$$k_s = \frac{\omega}{c_s} \ . \tag{24}$$

The solution to equation (19) is

$$\Phi(z) = A(k,\omega)\exp(\mathrm{i}\alpha z) + B(k,\omega)\exp(-\mathrm{i}\alpha z) \ , \tag{25}$$

and the solution to equation (22) is

$$\Psi(z) = C(k,\omega)\exp(\mathrm{i}\beta z) + D(k,\omega)\exp(-\mathrm{i}\beta z)\ , \tag{26}$$

where $A(k,\omega)$, $B(k,\omega)$, $C(k,\omega)$, and $D(k,\omega)$ are wave response coefficients that are determined later in this section. Use of the expressions in equations (9) and (10) now allows the displacements to be written as functions of the unknown constants as follows:

$$\begin{aligned} u_z(x,z,t) &= U_z(k,z,\omega)\exp(\mathrm{i}kx)\exp(\mathrm{i}\omega t) \\ &= \{\mathrm{i}\alpha[A(k,\omega)\exp(\mathrm{i}\alpha z) - B(k,\omega)\exp(-\mathrm{i}\alpha z)] \\ &\quad + \mathrm{i}k[C(k,\omega)\exp(\mathrm{i}\beta z) + D(k,\omega)\exp(-\mathrm{i}\beta z)]\}\exp(\mathrm{i}kx)\exp(\mathrm{i}\omega t) \end{aligned} \tag{27}$$

and

$$\begin{aligned} u_x(x,z,t) &= U_x(k,z,\omega)\exp(\mathrm{i}kx)\exp(\mathrm{i}\omega t) \\ &= \{\mathrm{i}k[A(k,\omega)\exp(\mathrm{i}\alpha z) + B(k,\omega)\exp(-\mathrm{i}\alpha z)] \\ &\quad - \mathrm{i}\beta[C(k,\omega)\exp(\mathrm{i}\beta z) - D(k,\omega)\exp(-\mathrm{i}\beta z)]\}\exp(\mathrm{i}kx)\exp(\mathrm{i}\omega t)\ . \end{aligned} \tag{28}$$

The normal stress at the top of the plate ($z = b$) is equal to the opposite of the pressure load created by the projector that acts on the plate surface and is expressed as

$$\tau_{zz}(x,b,t) = (\lambda + 2\mu)\frac{\partial u_z(x,b,t)}{\partial z} + \lambda\frac{\partial u_x(x,b,t)}{\partial x} = -p_0(x,b,t)\ ; \tag{29}$$

the tangential stress at the top of the plate is zero and is written as

$$\tau_{zx}(x,b,t) = \mu\left[\frac{\partial u_x(x,b,t)}{\partial z} + \frac{\partial u_z(x,b,t)}{\partial x}\right] = 0\ . \tag{30}$$

The normal stress at the bottom of the plate ($z = a$) is equal to zero, yielding

$$\tau_{zz}(x,a,t) = (\lambda + 2\mu)\frac{\partial u_z(x,a,t)}{\partial z} + \lambda\frac{\partial u_x(x,a,t)}{\partial x} = 0 \ , \tag{31}$$

and the tangential stress at the bottom of the plate is zero, resulting in

$$\tau_{zx}(x,a,t) = \mu\left[\frac{\partial u_x(x,a,t)}{\partial z} + \frac{\partial u_z(x,a,t)}{\partial x}\right] = 0 \ . \tag{32}$$

The applied load in equation (29) is an acoustic pressure that is modeled as a function at definite wavenumber and frequency and is expressed as

$$p_0(x,z,t) = P_0(\omega)\exp(ikx)\exp(i\omega t) \ , \tag{33}$$

where the wavenumber k is found using

$$k = \frac{\omega}{c_f}\sin(\theta) \ , \tag{34}$$

in which c_f is the compressional wavespeed of air (m/s) and θ is the angle of incidence of the projector with the z-axis (rad).

Assembling equations (1)-(34) and letting $b = 0$ yields the following four-by-four system of linear equations that models the structure:

$$\mathbf{Ax} = \mathbf{b} \ , \tag{35}$$

where the entries of equation (35) are

$$A_{11} = -\alpha^2\lambda - 2\alpha^2\mu - \lambda k^2 \ , \tag{36}$$

$$A_{12} = A_{11} \ , \tag{37}$$

$$A_{13} = 2k\beta\mu \ , \tag{38}$$

$$A_{14} = A_{13} \ , \tag{39}$$

$$A_{21} = -2\mu k\alpha \ , \tag{40}$$

$$A_{22} = -A_{21} \ , \tag{41}$$

$$A_{23} = \mu\beta^2 - \mu k^2 \ , \tag{42}$$

$$A_{24} = A_{23} \ , \tag{43}$$

$$A_{31} = A_{11}\exp(\mathrm{i}\alpha a) \ , \tag{44}$$

$$A_{32} = A_{11}\exp(-\mathrm{i}\alpha a) \ , \tag{45}$$

$$A_{33} = -A_{13}\exp(\mathrm{i}\beta a) \ , \tag{46}$$

$$A_{34} = A_{13}\exp(-\mathrm{i}\beta a) \ , \tag{47}$$

$$A_{41} = A_{21}\exp(\mathrm{i}\alpha a) \ , \tag{48}$$

$$A_{42} = -A_{21}\exp(-\mathrm{i}\alpha a) \ , \tag{49}$$

$$A_{43} = A_{23}\exp(\mathrm{i}\beta a) \ , \tag{50}$$

$$A_{44} = A_{23}\exp(-\mathrm{i}\beta a) \ , \tag{51}$$

$$b_{11} = -P_0(\omega) \ , \tag{52}$$

$$b_{21} = 0 \ , \tag{53}$$

$$b_{31} = 0 \ , \tag{54}$$

and

$$b_{41} = 0 \ . \tag{55}$$

From equations (35)-(55), the solution to the constants $A(k,\omega)$, $B(k,\omega)$, $C(k,\omega)$, and $D(k,\omega)$ can be calculated at each specific wavenumber and frequency from

$$\mathbf{x} = \mathbf{A}^{-1}\mathbf{b} \ . \tag{56}$$

Once these solutions are known, the transfer function between the wall motion in the z-direction at $z = a$ and the wall motion in the z-direction at $z = b$ is written in closed-form notation from equations (27) and (56) as

$$T(k,\omega) = \frac{U_z(k,a,\omega)}{U_z(k,b,\omega)} = \frac{4\alpha\beta k^2 \sin(\alpha h) + (\beta^2 - k^2)^2 \sin(\beta h)}{4\alpha\beta k^2 \sin(\alpha h)\cos(\beta h) + (\beta^2 - k^2)^2 \cos(\alpha h)\sin(\beta h)} \ . \tag{57}$$

The expression in equation (57) will first be used in the inverse method to estimate α and then to estimate β, both of which will ultimately be employed to calculate the mechanical properties of the material. This process is further described in the following sections.

INVERSE MODEL AT ZERO WAVENUMBER

The first step in the inverse process solves for the response at zero wavenumber (typically referred to as the broadside response) to determine the dilatational wavespeed. At zero wavenumber, the angle between the propagation direction of the insonification energy and the z-axis is zero and the response of the structure to broadside energy is comprised entirely of dilatational waves (i.e., no shear waves are excited at zero wavenumber). Moreover, the transfer function given in equation (57) reduces to

$$T(0,\omega) = \frac{1}{\cos(\alpha_1 h)} = T_1 = \frac{1}{R_1} \ , \tag{58}$$

where T_1 (or R_1) represents the data from the experiment with an insonification angle of zero (typically a frequency-dependent, complex number) and the subscript 1 denotes the first

experiment. Equation (58) can be expanded into real and imaginary parts and solved, resulting in a value for α_1 at every frequency for which a measurement is made. The solution to the real part of α_1 is

$$\mathrm{Re}(\alpha_1) = \begin{cases} \dfrac{1}{2h}\mathrm{Arccos}(s) + \dfrac{n\pi}{2h} & n \text{ even} \\ \dfrac{1}{2h}\mathrm{Arccos}(-s) + \dfrac{n\pi}{2h} & n \text{ odd} \end{cases}, \tag{59}$$

where

$$s = [\mathrm{Re}(R_1)]^2 + [\mathrm{Im}(R_1)]^2 - \sqrt{\left\{[\mathrm{Re}(R_1)]^2 + [\mathrm{Im}(R_1)]^2\right\}^2 - \left\{2[\mathrm{Re}(R_1)]^2 - 2[\mathrm{Im}(R_1)]^2 - 1\right\}}, \tag{60}$$

n is a non-negative integer, and capital A denotes the principal value of the inverse cosine function. The value of n is determined from the function s, which is a periodically varying cosine function with respect to frequency. At zero frequency, n is 0. Every time s cycles through π radians (180°), n is increased by 1. When the solution to the real part of α_1 is found, the solution to the imaginary part of α_1 is written as

$$\mathrm{Im}(\alpha_1) = \frac{1}{h}\log_e\left\{\frac{\mathrm{Re}(R_1)}{\cos[\mathrm{Re}(\alpha_1)h]} - \frac{\mathrm{Im}(R_1)}{\sin[\mathrm{Re}(\alpha_1)h]}\right\}. \tag{61}$$

The real and imaginary parts of α_1 from equations (59) and (61), respectively, are combined to yield the complex wavenumber. Because this measurement is made at zero wavenumber ($k \equiv 0$), α_1 is equal to the dilatational wavenumber. Thus, the dilatational wavespeed is expressed as

$$c_d = \frac{\omega}{[\mathrm{Re}(\alpha_1) + \mathrm{i}\,\mathrm{Im}(\alpha_1)]}. \tag{62}$$

To solve for the shear wavespeed, the specimen must be excited at a nonzero wavenumber as shown in the next section.

INVERSE MODEL AT NONZERO WAVENUMBER

The next step solves for the response at nonzero wavenumber to determine the shear wavespeed. The transfer function at the nonzero wavenumber is given in equation (57) and can be expressed for the nonzero angle of insonification as

$$T(k,\omega) = \frac{4\alpha_2\beta_2 k_2^2 \sin(\alpha_2 h) + (\beta_2^2 - k_2^2)^2 \sin(\beta_2 h)}{4\alpha_2\beta_2 k_2^2 \sin(\alpha_2 h)\cos(\beta_2 h) + (\beta_2^2 - k_2^2)^2 \cos(\alpha_2 h)\sin(\beta_2 h)} = T_2 = \frac{1}{R_2}, \qquad (63)$$

where T_2 (or R_2) represents the data from the experiment at the nonzero insonification angle (typically a frequency-dependent, complex number) and the subscript 2 denotes the second experiment. It is noted that α_2 in equation (63) is different from α_1 in equation (58), with this difference based on the k^2 term shown in equation (20), where the wavenumber α is defined. Due to the complexity of equation (63), there is no simple method for rewriting the equation as a function of β_2, which is the variable that is to be estimated. Rather, equation (63) is rewritten as

$$f(\beta_2) = 0 = 4\alpha_2\beta_2 k_2^2 \sin(\alpha_2 h)[\cos(\beta_2 h) - R_2] + (\beta_2^2 - k_2^2)^2 \sin(\beta_2 h)[\cos(\alpha_2 h) - R_2], \qquad (64)$$

where the problem now becomes finding the zeros of the right-hand side of equation (64) or, in the presence of actual data that contain noise, finding the relative minima of the right-hand side of this equation, with the purpose of determining which relative minimum corresponds to shear wave propagation and which relative minima are extraneous. Because equation (64) has a number of relative minima, zero-finding algorithms are not applied to this function, as they typically do not find all the minima locations and are highly dependent on initial guesses. The best method for locating all the minima is to plot the absolute value of the right-hand side of

equation (64) as a surface, with the real part of β_2 on one axis and the imaginary part of β_2 on the other axis. The value α_2 is determined from

$$\alpha_2 = \sqrt{k_d^2 - k_2^2} = \sqrt{\alpha_1^2 - k_2^2} \ , \tag{65}$$

so that equation (64) is a function of only (complex) β_2. Once this function is plotted, the minima can be easily identified and the corresponding value of $(\beta_2)_m$ at the location of the minima can be determined by examination of the minimum location — an approach that is sometimes referred to as the grid method. The shear wavenumber(s) and wavespeed(s) are then determined from

$$(k_s)_m = \sqrt{(\beta_2)_m^2 + k_2^2} \tag{66}$$

and

$$(c_s)_m = \frac{\omega}{(k_s)_m} \ , \tag{67}$$

where the subscript m denotes each minima value that was found by inspecting the surface formed from equation (64). Determination of the correct index of m that corresponds to shear wave propagation is presented in the next section.

DETERMINATION OF PROPERTIES FROM WAVESPEEDS

The process of determining the material properties from the wavespeeds begins with calculation of the Lamé constants from equations (13) and (14), which is expressed as

$$\mu_m = \rho(c_s)_m^2 \tag{68}$$

and

$$\lambda_m = \rho c_d^2 - 2\rho(c_s)_m^2 \ . \tag{69}$$

To determine the correct index m that corresponds to the actual wave propagation rather than to an extraneous solution, a third set of measurements is made at a nonzero incidence angle that is not equal to the angle used in the previous section. That is, the model in equation (63) is calculated from the estimated material properties, with a residual value established from this third set of measurements. Each m-indexed residual at a specific frequency is defined as

$$(\varepsilon_3)_m = \frac{4\alpha_3(\beta_3)_m k_3^2 \sin(\alpha_3 h) + [(\beta_3)_m^2 - k_3^2]^2 \sin[(\beta_3)_m h]}{4\alpha_3(\beta_3)_m k_3^2 \sin(\alpha_3 h)\cos[(\beta_3)_m h] + [(\beta_3)_m^2 - k_3^2]^2 \cos(\alpha_3 h)\sin[(\beta_3)_m h]} - \frac{1}{R_3}, \tag{70}$$

where

$$\alpha_3 = \sqrt{k_d^2 - k_3^2} = \sqrt{\alpha_1^2 - k_3^2} \tag{71}$$

and

$$(\beta_3)_m = \sqrt{(\beta_2)_m^2 + k_2^2 - k_3^2}\ , \tag{72}$$

with the subscript 3 denoting the third experiment. The smallest residual value corresponds to the correct value of index m and the correct values of the Lamé constants. Poisson's ratio is then calculated using

$$\upsilon = \frac{\lambda}{2(\mu + \lambda)}\ . \tag{73}$$

Young's modulus can be calculated from

$$E = \frac{2\mu(2\mu + 3\lambda)}{2(\mu + \lambda)}\ , \tag{74}$$

and the shear modulus from

$$G \equiv \mu\ . \tag{75}$$

NUMERICAL SIMULATION

The inverse measurement method presented here can be simulated by means of a numerical example that uses a soft rubberlike material with the following properties: Young's modulus E of $[(1e8 - i2e7) + (5e3f - i3e2f)]$ N/m^2, where f is frequency in Hertz; Poisson's ratio υ equal to 0.40 (dimensionless); density ρ equal to 1200 kg/m^3; and thickness h of 0.1 m. A compressional (acoustic) wave velocity of $c_f = 343$ m/s for air was used. All other parameters can be calculated from these values.

Insonification angles of 0°, 20°, and 40° are chosen to illustrate the technique, with three different amounts of additive noise used during the simulation: no additive noise, 1% additive noise, and 2% additive noise. Additive noise is included in the transfer function using the equation

$$T_e(\omega) = T(\omega) + e\{\mathrm{Re}[T(\omega)]\sigma_a + i\mathrm{Im}[T(\omega)]\sigma_b\} \ , \tag{76}$$

where e is the amount of additive noise added to the transfer function and σ_a and σ_b are random numbers with zero mean and a variance of one. The value e is also called the transfer function error value, and it represents the deviation of the transfer function from perfect data.

Figure 3 is a plot of the transfer functions of equation (57) at 0°, 20°, and 40° insonification angles versus frequency. The top plot illustrates the magnitude and the bottom plot presents the phase angle. Although the transfer functions shown are without additive noise, the transfer functions with additive noise were similar to those seen in this figure. Once the transfer functions are known (typically by measurement, but, in this report, by numerical simulation), the dilatational wavespeed can be estimated from equations (59)–(62).

Figure 4 is a plot of the function s versus frequency without additive noise, and figure 5 illustrates the actual dilatational wavespeed and the estimated dilatational wavespeed without additive noise, with 1% additive noise, and with 2% additive noise versus frequency. The top plot is the real component and the bottom plot is the imaginary component of the wavespeed.

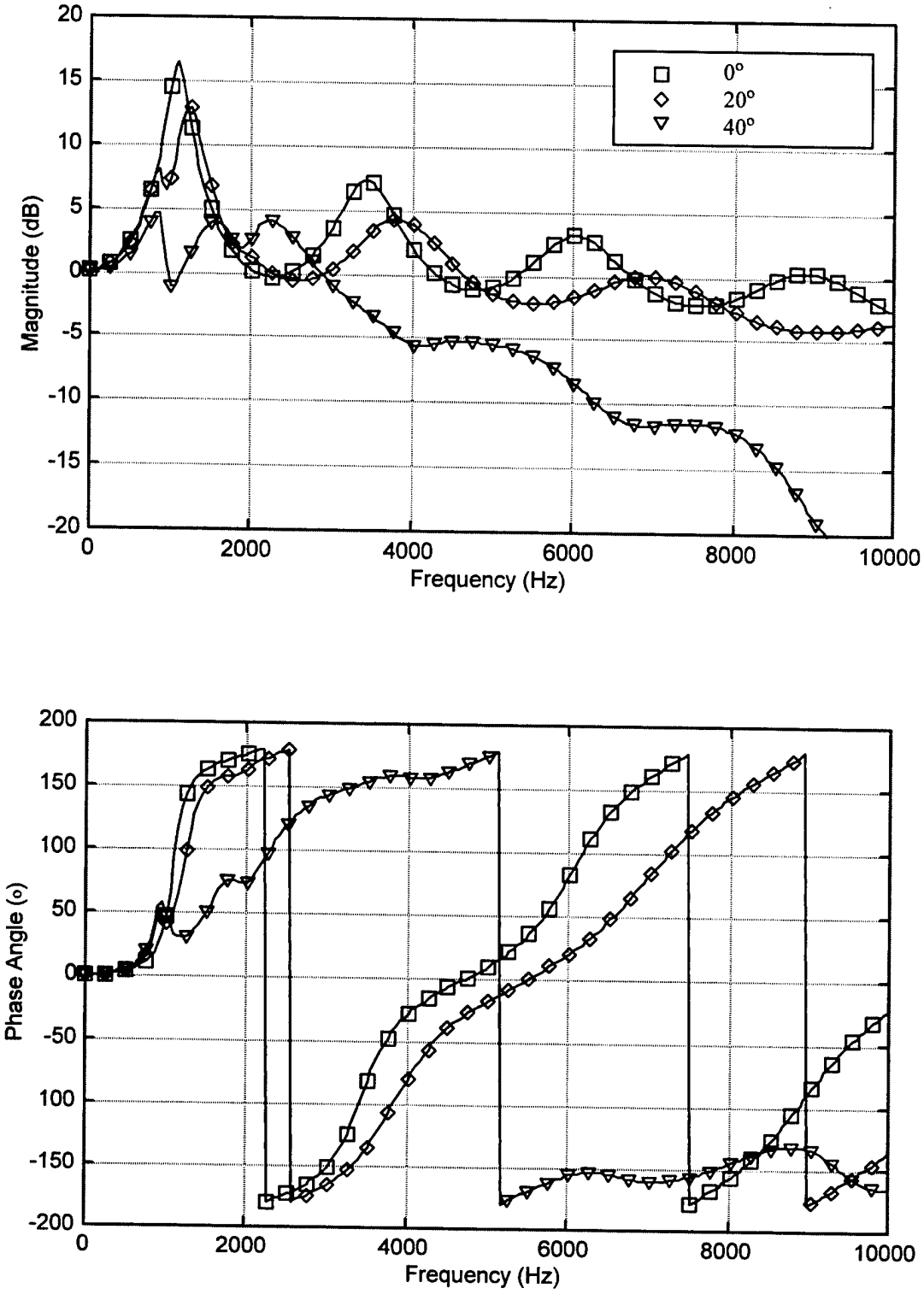

Figure 3. Transfer Function Versus Frequency

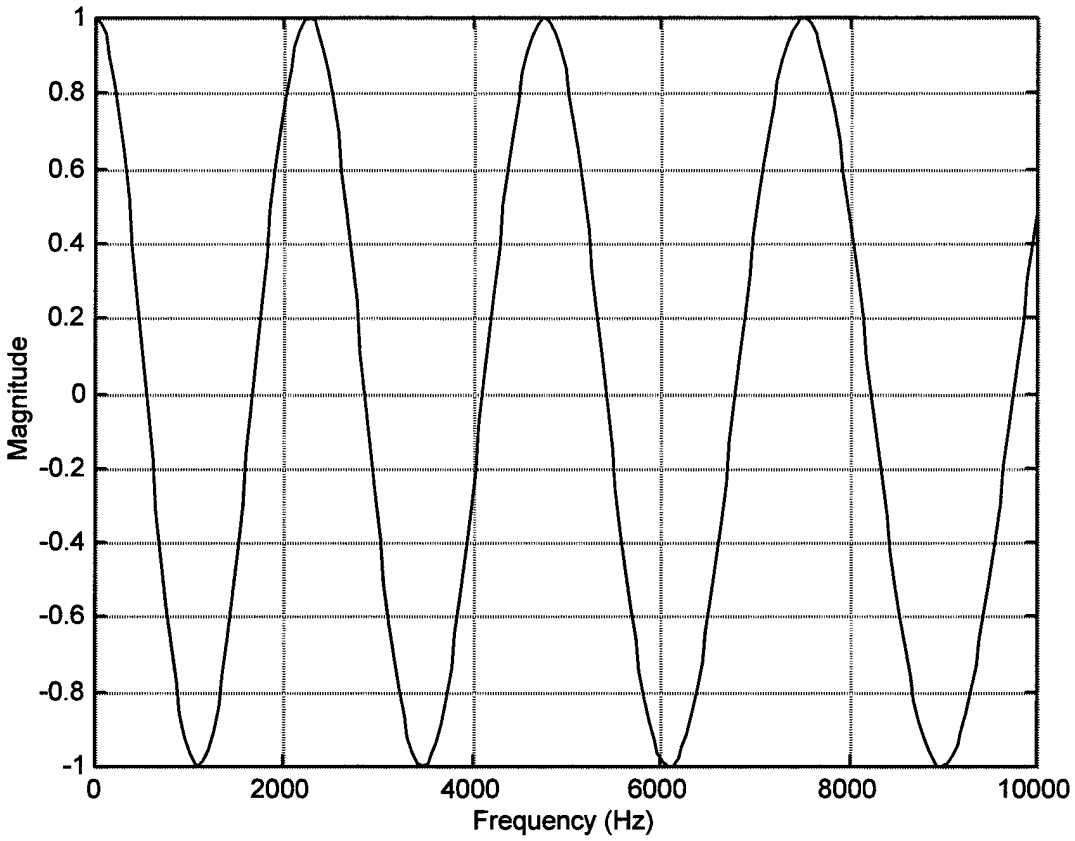

Figure 4. Function s Versus Frequency

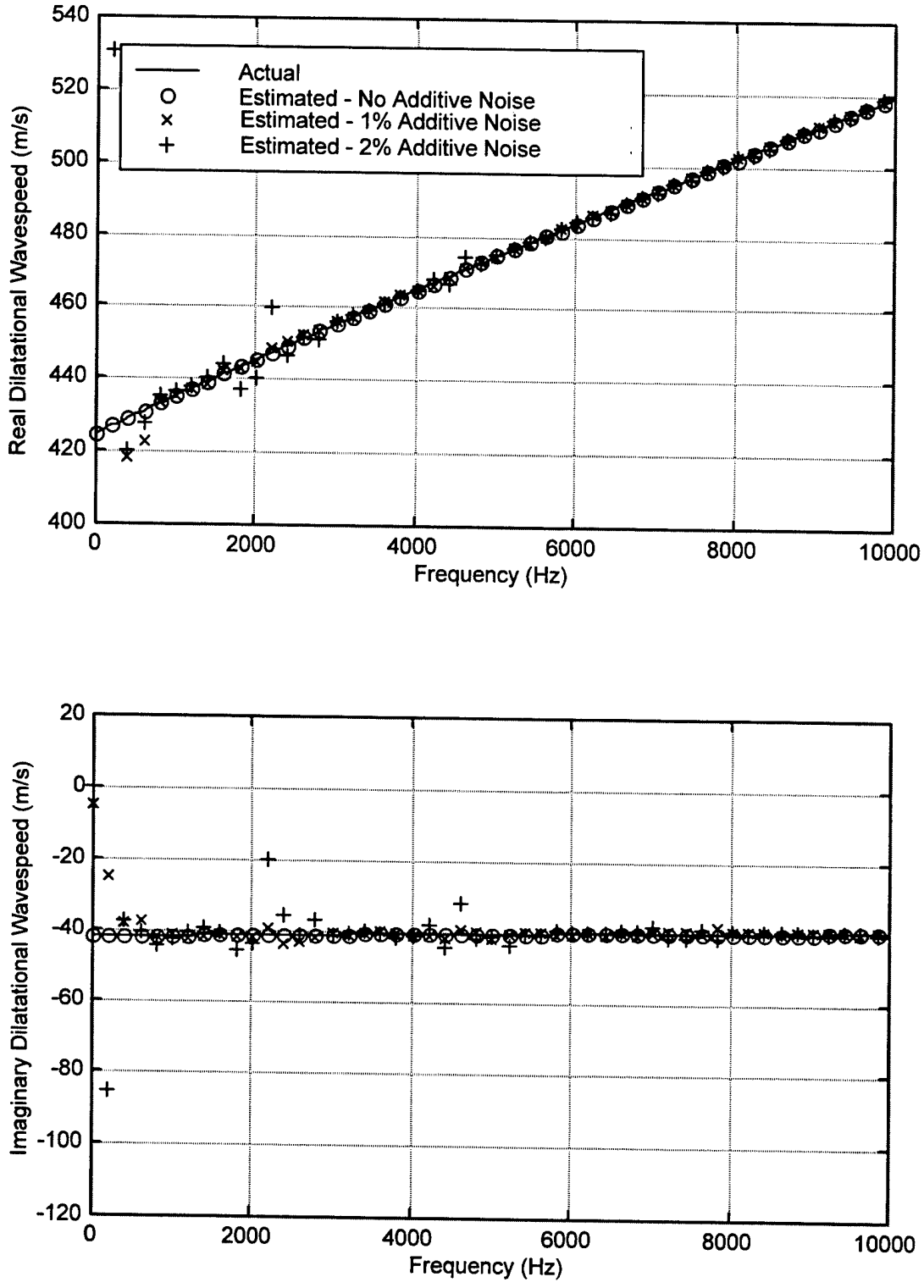

Figure 5. Actual and Estimated Dilatational Wavespeed Versus Frequency

Figure 6 plots the absolute value of the magnitude of the surface defined in equation (64) versus the real and imaginary components of β_2 at 1800 Hz without additive noise. The surface, discretized with 400 by 400 points, has its magnitude expressed in a decibel scale. Seven distinct local minima exist, with the first local minimum corresponding to $\beta_2 = 0$, which is a value that implies no shear wave propagation (a physically unrealizable condition at nonzero wavenumber). The other six local minima are labeled on the figure with bold numbers and are processed at a third measurement location according to equation (70).

The results for no additive noise are provided in table 1. As is evident, local minimum number 3 has the smallest residual value and corresponds to the shear wave propagation. The value for $(\beta_2)_3$ is equal to 60.9 + 5.9i compared to the actual value of β_2 which is 61.0 + 5.9i. The small difference between these two values can be attributed to the discretization of the surface as shown in the figure. Additionally, it is noted that the local minima numbered 4, 5, and 6 have an imaginary value almost equal to zero, which would correspond to a loss factor of zero. Most soft materials have moderate to large loss values, which means that these minima could be disregarded based on this criterion. The variable β_2 at 1800 Hz was next estimated using 1% and 2% additive noise, as shown in tables 2 and 3, respectively. These results illustrate that the residual method is effective when noise is present in the data.

Figure 7 is a plot of the actual shear wavespeed and the estimated shear wavespeed without additive noise, with 1% additive noise, and with 2% additive noise versus frequency. The top plot presents the real component and the bottom part shows the imaginary component of the wavespeed. The figure was constructed by repeating the measurement process shown in figure 6 at each specified frequency.

Figure 8 plots the actual shear modulus and the estimated shear modulus without additive noise, with 1% additive noise, and with 2% additive noise versus frequency. The top plot represents the real component and the bottom part shows the loss factor of the shear modulus.

Figure 9 is a plot of the actual Young's modulus and the estimated Young's modulus without additive noise, with 1% additive noise, and with 2% additive noise versus frequency. The top plot is the real component and the bottom part is the loss factor of the Young's modulus.

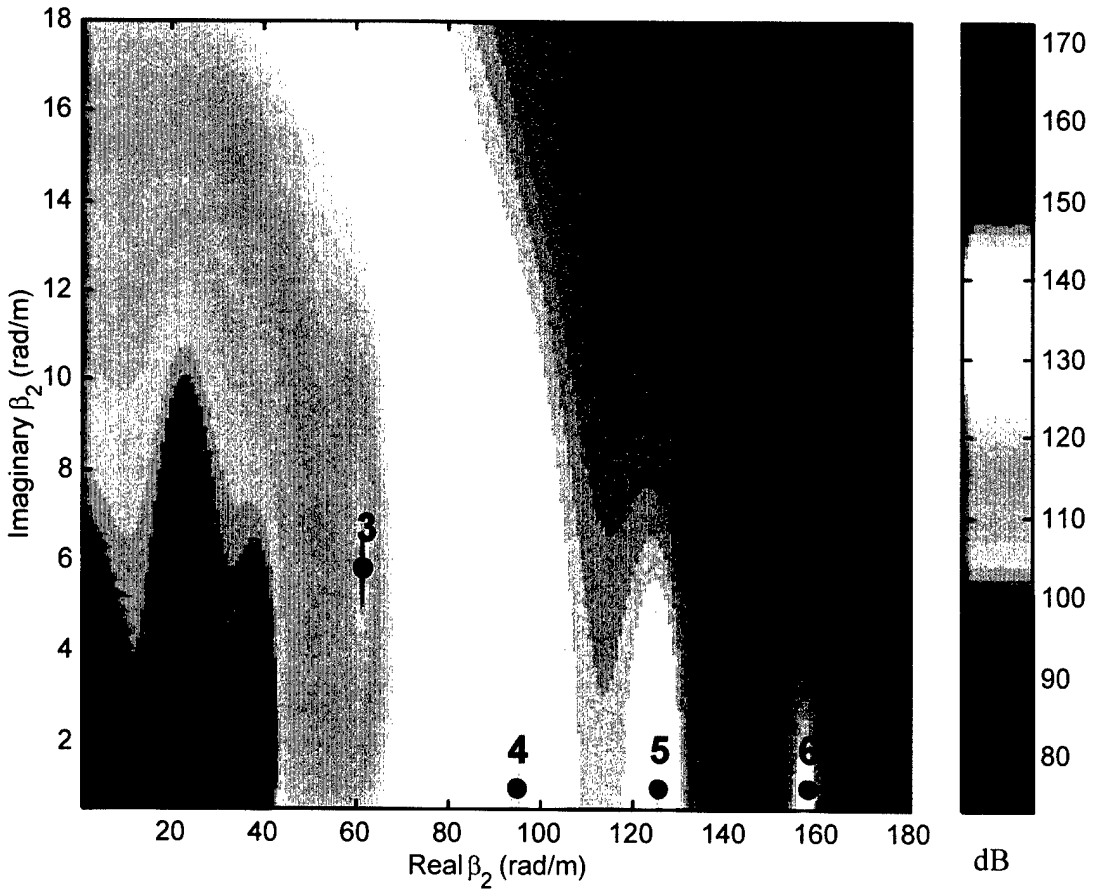

Figure 6. Magnitude of Surface Versus Real and Imaginary β_2 at 1800 Hz

Table 1. Values of $(\beta_2)_m$ and $(\varepsilon_3)_m$ at the Local Minima Without Additive Noise

Local Minima Number *m*	**Value of $(\beta_2)_m$**	**Residual $(\varepsilon_3)_m$ (Equation (70))**
1	22.1 + 5.2i	0.302
2	38.4 + 2.5i	2.006
3	60.9 + 5.9i	0.001
4	94.3 + 0.5i	0.506
5	125.1 + 0.6i	0.335
6	157.4 + 0.5i	0.378

Table 2. Values of $(\beta_2)_m$ and $(\varepsilon_3)_m$ at the Local Minima with 1% Additive Noise

Local Minima Number *m*	**Value of $(\beta_2)_m$**	**Residual $(\varepsilon_3)_m$ (Equation (70))**
1	22.1 + 5.2i	0.275
2	39.3 + 2.2i	2.170
3	60.9 + 6.3i	0.045
4	94.3 + 0.5i	0.516
5	125.0 + 0.6i	0.312
6	157.4 + 0.5i	0.371

Table 3. Values of $(\beta_2)_m$ and $(\varepsilon_3)_m$ at the Local Minima with 2% Additive Noise

Local Minima Number *m*	**Value of $(\beta_2)_m$**	**Residual $(\varepsilon_3)_m$ (Equation (70))**
1	22.1 + 5.3i	0.344
2	38.4 + 2.7i	1.979
3	60.9 + 5.2i	0.009
4	94.3 + 0.5i	0.519
5	125.0 + 0.5i	0.361
6	157.4 + 0.5i	0.398

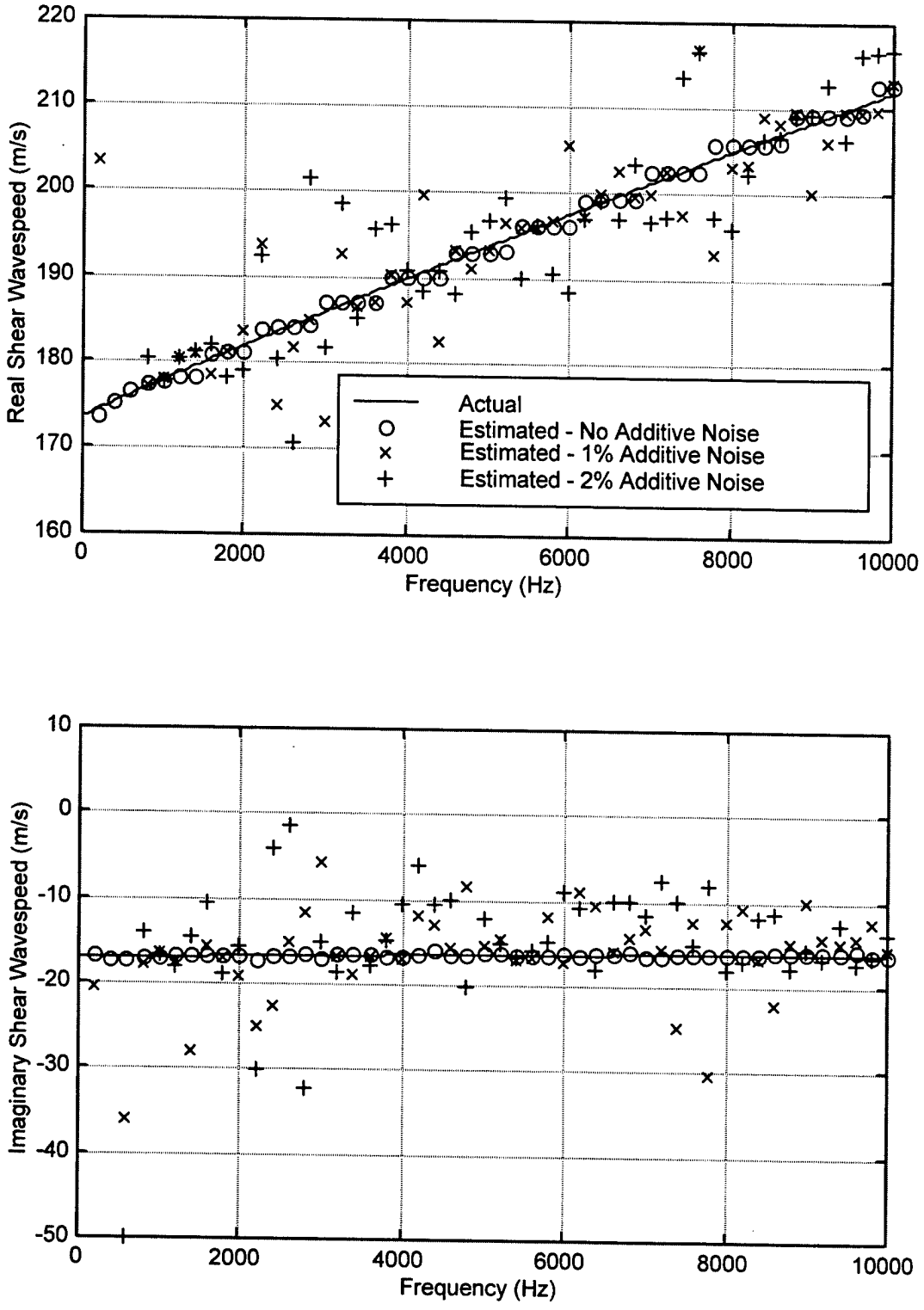

Figure 7. Actual and Estimated Shear Wavespeed Versus Frequency

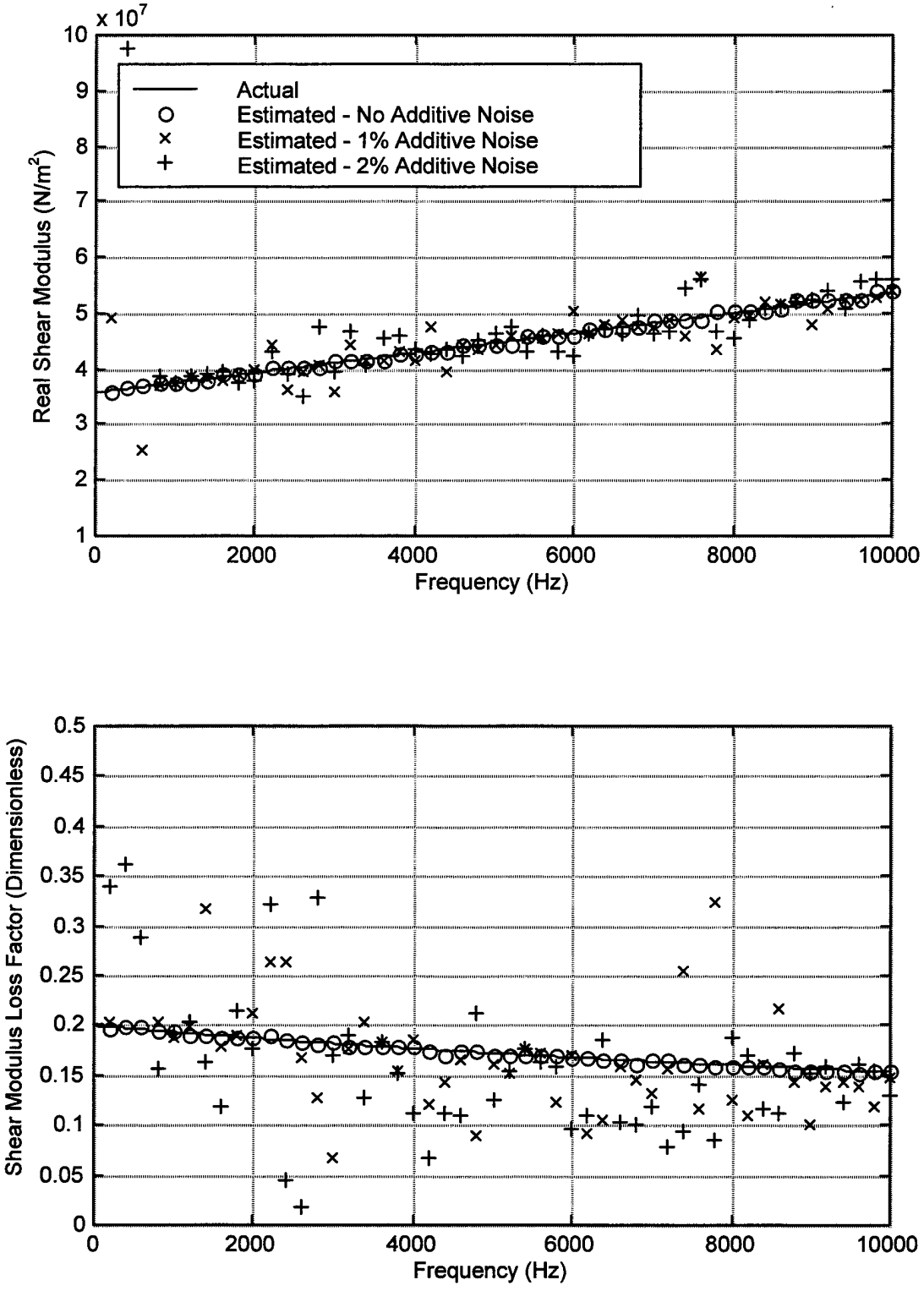

Figure 8. Actual and Estimated Shear Modulus Versus Frequency

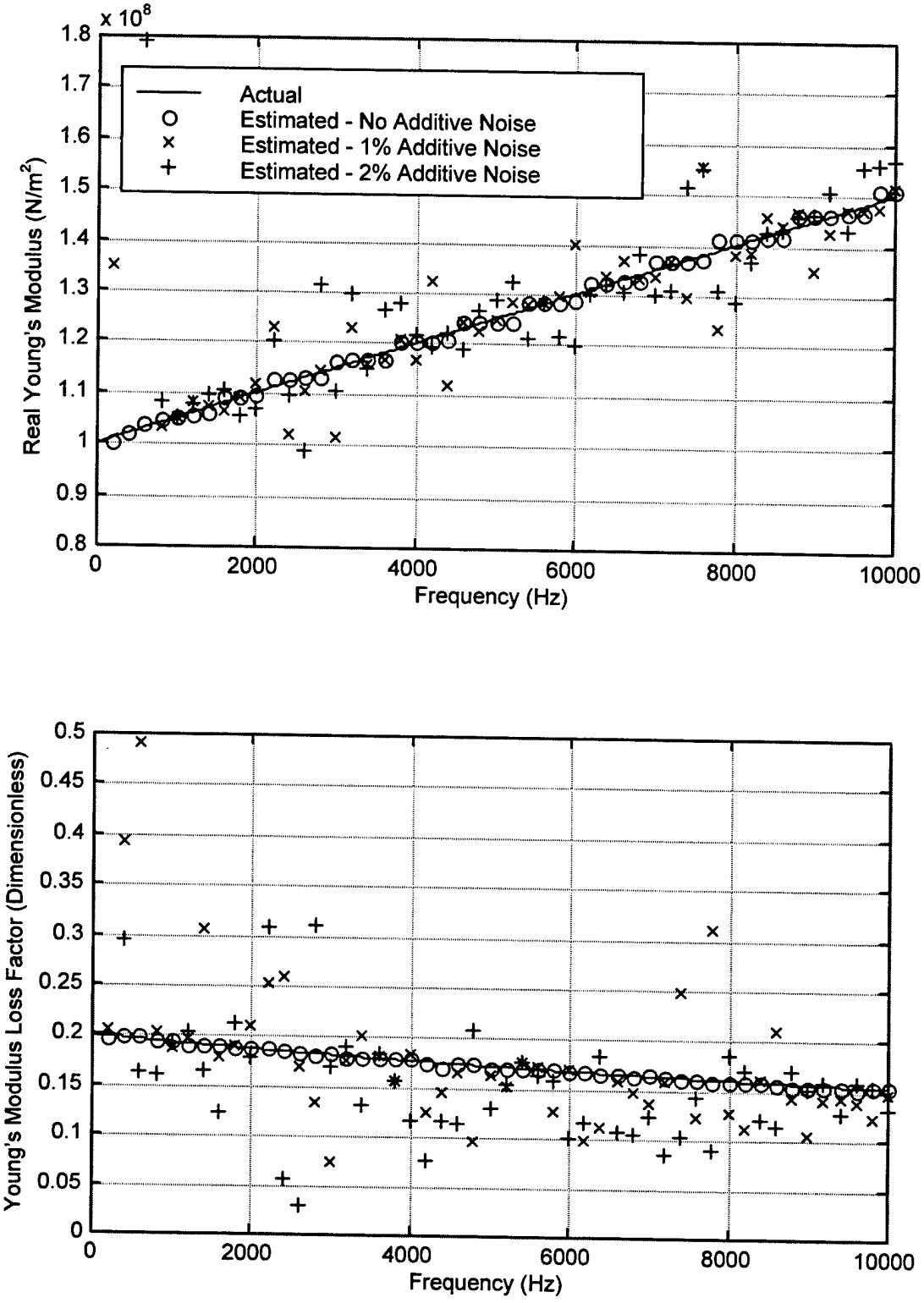

Figure 9. Actual and Estimated Young's Modulus Versus Frequency

Figure 10 illustrates the actual real Poisson's ratio and the estimated real Poisson's ratio without additive noise, with 1% additive noise, and with 2% additive noise versus frequency. Because the numerical example is formulated using a Poisson's ratio that is strictly real, no imaginary component is shown in this plot. Imaginary values of Poisson's ratio are possible and have been shown to theoretically exist.[17]

Finally, the additive noise versus the parameter estimation error is shown in table 4. Parameter estimation error was computed from

$$\theta = \frac{1}{N}\sum_{n=1}^{N}\frac{\left|\kappa_{est}(\omega_n) - \kappa_{act}(\omega_n)\right|}{\left|\kappa_{act}(\omega_n)\right|}, \tag{77}$$

where θ is the parameter estimation error, $\kappa_{est}(\omega_n)$ is the estimated value of the parameter at the nth frequency value, $\kappa_{act}(\omega_n)$ is the actual value of the parameter at the nth frequency value, and N is the total number of frequencies at which an estimate was computed. It is noted that at very low frequencies the routine did not produce a realistic estimate of the parameters, and thus these estimates are not included in the table.

Table 4 shows that all the parameters are being estimated accurately with the inverse technique. At 1% additive noise, the maximum error in the wavespeeds is 2.6% and the maximum error of the material properties is 5.1%. At 2% additive noise, the maximum error in the wavespeeds is 3.4% and the maximum error of the material properties is 6.8%. Poisson's ratio has a parameter estimation error of 1.4% when the transfer functions have 2% additive noise, which is remarkably low for a parameter that is historically very difficult to measure.

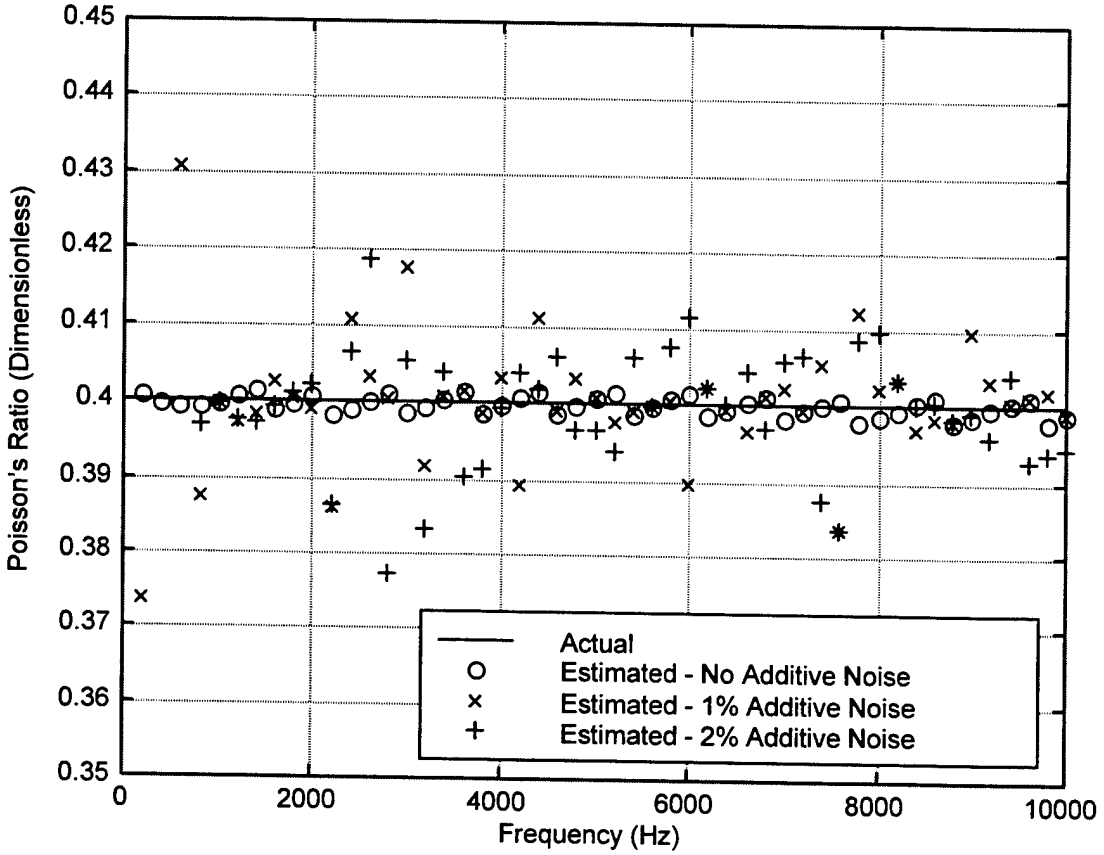

Figure 10. Actual and Estimated Poisson's Ratio Versus Frequency

Table 4. Additive Noise Versus Parameter Estimation Error

Parameter	Additive Noise	Parameter Estimation Error
c_d	0	~0
c_d	0.010	0.014
c_d	0.020	0.016
c_s	0	0.004
c_s	0.010	0.026
c_s	0.020	0.034
G	0	0.007
G	0.010	0.051
G	0.020	0.068
E	0	0.007
E	0.010	0.047
E	0.020	0.063
υ	0	0.002
υ	0.010	0.010
υ	0.020	0.014

CONCLUSIONS

In this report, a theoretical method for estimating the mechanical properties of slab-shaped materials subjected to insonification has been derived. Measurement of the transfer functions of acceleration across the plate at three different insonification angles shows that the dilatational wavespeed, shear wavespeed, Young's modulus, shear modulus, and Poisson's ratio can be accurately determined. Moreover, the technique is relatively immune to noise mechanisms that are sometimes present in the measurements.

It is recommended that actual measurement data be used to evaluate the effectiveness of the inverse method.

REFERENCES

1. D. M. Norris Jr. and W. C. Young, "Complex Modulus Measurements by Longitudinal Vibration Testing," *Experimental Mechanics*, vol. 10, 1970, pp. 93-96.

2. W. M. Madigosky and G. F. Lee, "Improved Resonance Technique for Materials Characterization," *Journal of the Acoustical Society of America*, vol. 73, no. 4, 1983, pp. 1374-1377.

3. S. O. Oyadiji and G. R. Tomlinson, "Determination of the Complex Moduli of Viscoelastic Structural Elements by Resonance and Non-Resonance Methods," *Journal of Sound and Vibration*, vol. 101, no. 3, 1985, pp. 277-298.

4. S. L. Garrett, "Resonant Acoustic Determination of Elastic Moduli," *Journal of the Acoustical Society of America*, vol. 88, no. 1, 1990, pp. 210-220.

5. J. L. Buchanan, "Numerical Solution for the Dynamic Moduli of a Viscoelastic Bar," *Journal of the Acoustical Society of America*, vol. 81, no. 6, 1987, pp. 1775-1786.

6. T.-K. Ahn and K.-J. Kim, "Sensitivity Analysis for Estimation of Complex Modulus of Viscoelastic Materials by Non-Resonance Method," *Journal of Sound and Vibration*, vol. 176, no. 4, 1994, pp. 543-561.

7. A. J. Hull, "An Inverse Method to Measure the Axial Modulus of Composite Materials Under Tension," *Journal of Sound and Vibration*, vol. 195, no. 4, 1996, pp. 545-551.

8. F. M. Guillot and J. Jarzynski, "A New Method for Measuring the Bulk Modulus of Compliant Acoustic Materials," *Journal of Sound and Vibration*, vol. 233, no. 5, 2000, pp. 929-934.

9. T. Pritz, "Transfer Function Method for Investigating the Complex Modulus of Acoustic Materials: Rod-Like Specimen," *Journal of Sound and Vibration*, vol. 81, 1982, pp. 359-376.

10. B. J. Dobson, "A Straight-Line Technique for Extracting Modal Properties from Frequency Response Data," *Mechanical Systems and Signal Processing*, vol. 1, 1987, pp. 29-40.

11. R. L. Willis, T. S. Stone, Y. H. Berthelot, and W. M. Madigosky, "An Experimental-Numerical Technique for Evaluating the Bulk and Shear Dynamic Moduli of Viscoelastic Materials," *Journal of the Acoustical Society of America*, vol. 102, no. 6, 1997, pp. 3549-3555.

12. R. L. Willis, L. Wu, and Y. H. Berthelot, "Determination of the Complex Young and Shear Dynamic Moduli of Viscoelastic Materials," *Journal of the Acoustical Society of America*, vol. 109, no. 2, 2001, pp. 611-621.

13. S. I. Roklin and W. Wang, "Measurements of Elastic Constants of Very Thin Anisotropic Plates," *Journal of the Acoustical Society of America*, vol. 94, no. 5, 1993, pp. 2721-2730.

14. V. Marchand, J. Authesserre, J. Pouyet, and C. Bacon, "Determination of the Elastic Constants of Materials, in the Form of Plates, by a Free Vibration Method," *Journal of Sound and Vibration*, vol. 194, no. 4, 1996, pp. 497-512.

15. F. Moussu and M. Nivoit, "Determination of Elastic Constants of Orthotropic Plates by a Modal Analysis/Method of Superposition," *Journal of Sound and Vibration*, vol. 165, no. 1, 1993, pp. 149-163.

16. W. Madigosky and R. Fiorito, "Modal Resonance Analysis of Acoustic Transmission and Reflection Losses in Viscoelastic Plates," *Journal of the Acoustical Society of America*, vol. 65, no. 5, 1979, pp. 1105-1115.

17. T. Pritz, "Frequency Dependencies of Complex Moduli and Complex Poisson's Ratio of Real Solid Materials," *Journal of Sound and Vibration*, vol. 214, no. 1, 1998, pp. 83-104.

INITIAL DISTRIBUTION LIST

Addressee	No. of Copies
Office of Naval Intelligence (ONI 241 – J. Zilius, T. Morgan; ONI 263 – S. Brown (2))	4
Office of Naval Research (ONR 321 – R. Elswick; ONR 333 – K. Ng)	2
Defense Technical Information Center	2
Center for Naval Analyses	1